Hindawi
Advances in Civil Engineering
Volume 2019, Article ID 9701324, 13 pages
https://doi.org/10.1155/2019/9701324

Research Article

Numerical Study on Deformation Capacity of Steel Plate Reinforced Concrete Shear Walls

Zhi Zhou,[1] **Jiang Qian**,[1] **and Wei Huang**[2]

[1]*State Key Laboratory of Disaster Reduction in Civil Engineering, Tongji University, Shanghai 200092, China*
[2]*Hubei Key Laboratory of Theory and Application of Advanced Materials Mechanics, School of Science, Wuhan University of Technology, Wuhan 430070, China*

Correspondence should be addressed to Wei Huang; whuang@whut.edu.cn

Received 14 March 2019; Revised 20 June 2019; Accepted 21 July 2019; Published 14 August 2019

Academic Editor: M. Shahria Alam

Steel plate reinforced concrete (SPRC) shear wall consists of steel plate encased in the concrete, in which the material advantages of both concrete and steel are utilized. The lateral resistance and deformation capacity of the shear wall are greatly improved. This paper investigates the deformation capacity of the SPRC shear wall under cyclic loads. A nonlinear 3-D finite element model in ABAQUS was developed and validated against published experimental results. Then, a parametric study was conducted to obtain the yield and ultimate rotation of SPRC shear walls with flexural failure. By statistical analyses, formulas for the yield and ultimate rotation of SPRC shear wall were proposed.

1. Introduction

Steel plate reinforced concrete (SPRC) shear wall consists of steel plate encased in the concrete wall as shown in Figure 1 [1]. Concrete on two sides of steel plate can prevent it from local buckling, and the shear yielding mechanism of steel plate can result in more stable hysteretic loops for shear wall [2]. This type of combination of concrete and steel plate can be utilized to change the potential brittle shear failure of RC shear wall to a ductile failure, while the stiffness and strength of the shear wall can also be significantly improved. Therefore, SPRC composite walls are generally used in cases where shear walls are designed to resist extreme lateral loads under earthquakes.

Experimental studies have been conducted by many researchers. Zhao and Astaneh-Asl [3] tested a series of composite shear walls and found them rather promising with a better capacity of energy dissipation. Gan et al. [4] conducted cyclic tests of 16 SPRC shear walls and investigated the effects of shear span ratio, the thickness of concrete and steel plate, and shear connectors between concrete and steel plate on the seismic behavior of shear walls. It shows that thicker concrete can provide more confinement to the steel plate and yield a more ductile failure and the shear studs can enhance the strength and ductility of SPRC shear wall. According to Wu [5], experimental results suggest that the increase of the steel plate ratio can significantly improve the strength of the SPRC shear wall but has a limited effect on its ductility. The strength and ductility of the SPRC shear wall are affected by the concrete thickness and boundary members. Jiang [6] tested 9 composite shear walls with different configurations under high axial load. It was concluded that the encased steel plate can greatly improve the flexural capacity of the shear wall and its deformation capacity degrades when designed axial load ratio exceeds 0.5. Zhu [7] tested 8 SPRC shear walls and 2 steel reinforced shear walls with a shear span ratio of 2.0. The SPRC shear walls were found to have a better capacity of energy dissipation than steel-reinforced concrete shear wall. And the energy dissipation capacity of SPRC shear walls can be improved by either increasing the reinforcement ratio or the rebar space of the wall web. It was pointed out that the steel plate and concrete can deform coordinately with the shear studs and tie bars in the test. Based on cyclic tests of 16 composite shear walls, Wang et al. [8] proposed a hysteretic model for SPRC shear walls.

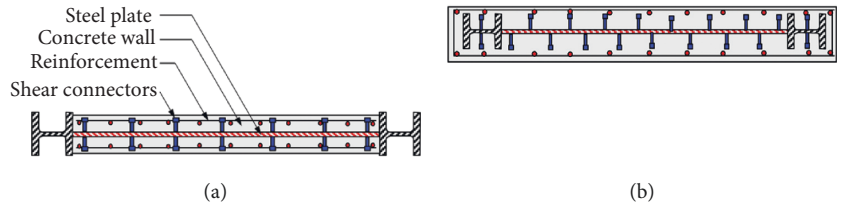

Figure 1: SPRC shear wall.

Numerical modelling has been carried out by researches to better understand the behavior of SPRC shear walls. Rahnavard et al. [9] conducted numerical analysis on different types of composite steel-concrete shear walls to study their hysteretic response, frame drift, and dissipated energy in Abaqus. The models involve concrete with and without gap to steel frame on one side and two sides of steel plate. It was concluded that the concrete on two sides of the steel plate has the highest shear capacity and lowest drift. Concrete layers on both sides of the steel plate can completely prevent steel plate buckling. A numerical model by OpenSees was developed by Wang et al. [10] to study the cyclic behavior of SPRC composite shear walls. This work identified the effects of steel plate ratio, axial load ratio, concrete strength, and reinforcement ratio on the cyclic behavior of SPRC shear wall.

Although a number of experimental and numerical studies have been reported to investigate the general behavior of the SPRC shear wall, few of them illustrate the prediction of the deformation capacity of SPRC shear wall. Since displacement-based design has been a common approach to seismic design, the yield and ultimate displacement of the SPRC shear wall are critical indices to determine its performance levels. The main objective of this study is to develop an efficient nonlinear 3-D finite element model to investigate the deformation of the SPRC shear wall under cyclic loads. ABAQUS was used in the analysis. Based on the finite element model which was validated against published test results, a parametric study of the SPRC shear wall with flexural failure was performed. Statistical analyses were utilized to propose formulas for yield rotation and ultimate rotation of SPRC shear walls.

2. Finite Element Modelling

Finite element software ABAQUS was used to simulate the behavior of SPRC shear walls. The main modelling approach is described as follows.

2.1. Modelling Approach. The SPRC composite shear wall studied in this paper is composed of four parts, concrete, structural steel, steel plate, longitudinal, and transverse reinforcement bars in wall web and boundary columns. The modelling of different parts of the SPRC shear wall is shown in Figure 2. Since structural steel and stirrups can provide different levels of confinement to concrete, the concrete part is divided into three zones accordingly, which are highly confined concrete, partially confined concrete, and unconfined

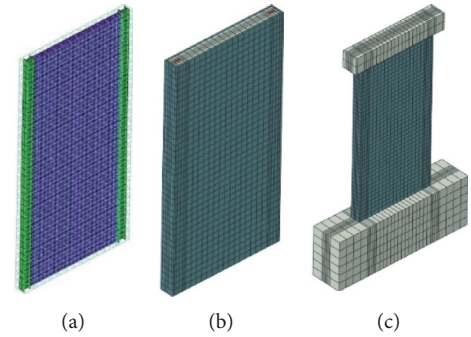

Figure 2: Modelling of the SPRC shear wall. (a) Structural steel, steel plate, and reinforcements. (b) Concrete. (c) The whole FE model.

concrete with different states of confinement. The highly confined concrete is taken from the web of the structural steel to the midwidth of each flange outstand. The unconfined concrete is taken from the centerline of the longitudinal reinforcement to the concrete cover. The partially confined concrete is the remaining part without any confinement, as shown in Figure 3 [11]. Their concrete model will be considered in different ways, which will be illustrated hereinafter.

2.2. Finite Element Type and Modelling of Interfaces. The concrete was modelled by the 3-D 8-node solid elements with reduced integration C3D8R. The steel plate was modelled by using the 4-node doubly curved shell elements with reduced integration S4R. The 2-node linear displacement truss elements were used to model the steel rebars. Well-distributed studs welded to the steel plate can almost assure the coworking of concrete and steel plate [4]. Additionally, high-strength steel wires that pass through the reserved holes in steel plate is tied to the transverse rebars in concrete wall web to strengthen the connection between concrete and steel plate. As the tests show [7], these configurations can well control the concrete and steel plate to deform together. Thus, the possible sliding between concrete and steel plate is ignored. The steel plate, structural steel, and reinforcements are embedded into the concrete using the *Embedded Constraint option in ABAQUS, assuming a perfect bond.

2.3. Material Modelling of Concrete. Concrete was modelled using the damaged plasticity model for concrete (CDP model) implemented in ABAQUS. The concrete strength and ductility under the confinement of steel and reinforcements are considerably improved. As illustrated by

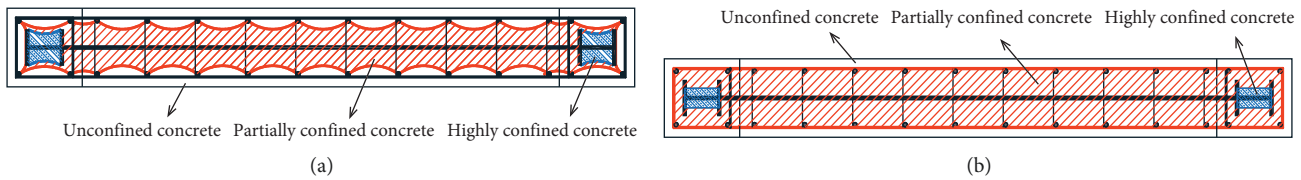

Figure 3: (a) Confinement zones in concrete and (b) simplified model.

Ellobody and Young [12], the CDP model may not be able to accurately simulate the compressive behavior of concrete under a high level of confinement. In this case, a confined concrete model needs to be developed. The input concrete compressive strength f_c will be taken as the unconfined concrete cylinder compressive strength f_{c0}, while the corresponding concrete strain ε_c will be taken as the confined strain ε_{cc}. According to Yu et al. [13], parameters that control the yield surface and flow rule are altered for partially and highly confined concrete, respectively. For highly confined concrete, $K_c = 0.725$ and $\psi = 56^\circ$. For partially confined concrete, $K_c = 0.667$ and $\psi = 42^\circ$. To improve the convergence speed, a viscosity parameter μ equal to 0.001 is introduced.

2.3.1. Unconfined Concrete. The concrete compressive strain ε_c is taken as ε_{c0}, which is the unconfined concrete strain corresponding to the unconfined concrete strength f_{c0}, taken as 0.003 as recommended by the fib model code for concrete structures [14].

2.3.2. Partially Confined Concrete. The compressive strain ε_c of confined concrete can be determined by using equation (1), proposed by Mander et al. [15] and improved by Denavit et al. [16]:

$$\varepsilon_c = \varepsilon_{c0}\left(1 + 5\left(K - 1\right)\right), \tag{1}$$

$$K = 1 + Af_l\left(0.1 + \frac{0.9}{1 + Bf_l}\right), \tag{2}$$

$$A = 6.8886 - \left(0.6069 + 17.275r\right)e^{-4.989r}, \tag{3}$$

$$B = \frac{4.5A}{5\left(0.9849 - 0.6306e^{-3.8939r}\right) - 0.1A} - 5, \tag{4}$$

$$f_l = \frac{f_{l1} + f_{l2}}{2f_{c0}}, \tag{5}$$

$$r = \frac{f_{l1}}{f_{l2}}, \quad f_{l1} \le f_{l2}, \tag{6}$$

where f_l is the equivalent lateral confining pressure and f_{l1} and f_{l2} are the lateral confining pressures imposed by the reinforcement bars with different directions, respectively, as given by Mander et al. [15].

2.3.3. Highly Confined Concrete. High confinement of concrete is provided by the steel and reinforcements. The lateral confining pressure (f'_{ly}) imposed by the flange of the steel is given by Huang et al. [17]:

$$f''_{ly} = K_e f''_{ly}, \tag{7}$$

$$f''_{ly} = \frac{f_{ys}t^2}{\sqrt{9l^4 + 3l^2t^2}}, \tag{8}$$

$$K_e = \frac{\left(L - h\right)\left(H - 2t\right) - \left(1/3\right)\left(H - 2t\right)^2}{\left(L - h\right)\left(H - 2t\right)}, \tag{9}$$

where f_{ys} is the yield strength of the steel, L is the flange length, H is the web length, and t is the flange thickness of the steel. The confined strain ε_c of the highly confined concrete can be determined by the lateral confining pressure imposed by the reinforcements and steel in different directions.

The model proposed by Popovics [18] and Collins [19] was adopted to simulate the concrete behavior in compression. The compressive stress f_c and strain ε_c relation of the concrete is defined as follows:

$$\sigma_c = \frac{f'_c\lambda\left(\varepsilon_c/\varepsilon'_c\right)}{\lambda - 1 + \left(\varepsilon_c/\varepsilon'_c\right)^{\lambda d}}, \tag{10}$$

$$\lambda = \frac{E_c}{E_c - \left(f'_c/\varepsilon'_c\right)}, \tag{11}$$

$$\begin{cases} d = 1, & \dfrac{\varepsilon_c}{\varepsilon'_c} \le 1, \\ d = 0.67 + \dfrac{f'_c}{62} \ge 1, & \dfrac{\varepsilon_c}{\varepsilon'_c} > 1, \end{cases} \tag{12}$$

where f_c is the peak compressive strength of concrete, λ is the curve-fitting factor, E_c is the initial tangent modulus, ε_0 is the strain when σ_c reaches f_c, and d is the factor which controls the slope of the stress-strain curve.

The initial Young's modulus of concrete is reasonably calculated using equation (13) given by the ACI Specification [20]. Poisson's ratio of concrete is taken as 0.2:

$$E_c = 4730\sqrt{f_c}. \tag{13}$$

Under uniaxial tension, the stress-strain response follows a linear elastic relationship until reaching the value of the failure stress. The tensile failure stress was assumed to be $0.395f_{cu}^{\ 0.55}$ where f_{cu} is the cubic compressive strength of concrete. The softening stress-strain response, past the maximum tensile stress, was represented by a linear line defined by the fracture energy and crack bandwidth, as

shown in Figure 4. The fracture energy G_f in N/mm (energy required to open a unit area of crack) was taken as equation (14) as recommended by the Fib Code [14]:

$$G_f = 73 \cdot (f_c)^{0.18}. \quad (14)$$

The concrete damaged plasticity model assumes that the reduction of the elastic modulus is given in terms of a scalar degradation variable d as in equation (15), where E_0 is the initial modulus. Figure 5 shows the stress-strain relation for cyclic compressive loading:

$$E = (1 - d)E_0. \quad (15)$$

The stiffness degradation variable d is a function of the stress state and the uniaxial damage variables d_t and d_c. According to Birtel and Mark [21], the damage variables d_t and d_c can be calculated by assuming a linear relation between plastic strain and inelastic strain:

$$d_c = 1 - \frac{\sigma_c E_c^{-1}}{\varepsilon_c^{pl}\left(1/b_c - 1\right) + \sigma_c E_c^{-1}}, \quad (16)$$

$$d_t = 1 - \frac{\sigma_t E_t^{-1}}{\varepsilon_t^{pl}\left(1/b_t - 1\right) + \sigma_t E_t^{-1}}, \quad (17)$$

where $b_c = 0.7$ and $b_t = 0.1$, suggested by Birtel and Mark [21]. ε_c^{pl} and ε_t^{pl} are the compressive and tensile plastic strain of concrete, respectively.

2.4. Validation of Finite Element Model. To validate the proposed finite element model, numerical models of 9 SPRC shear walls with different shear span ratios were developed. The results of the numerical analyses were compared with that of the tests to illustrate the accuracy of the modelling method. The detailed parameters of the specimens are listed in Table 1.

The load-displacement curves of the FEAs are compared with those of the tests in Figure 6. The softening of some specimens with a shear span ratio of 1.5 is not in good agreement with the test because the buckling of the steel plate at middle height is not well predicted in the numerical analyses. Even though the steel plate and concrete can almost deform together, the possible sliding between steel plate, reinforcement, and concrete will affect the unloading and reloading path of the cyclic behavior, as well as the idealization of the steel model. After all, the pinching effect, strength, and stiffness degradation are well predicted in most cases. The corresponding strengths and ductility ratios are listed in Tables 2 and 3. The equivalent energy method is adopted to obtain the yield point in the skeleton curve, and the ultimate displacement is taken as the displacement corresponding to the lateral force that decreases to 85% of the peak force. The strength and deformation capacities of the shear wall under cyclic loads are predicted with acceptable accuracy. It is concluded that well agreement between tests and numerical analyses is achieved.

Two failure modes were observed in the test and confirmed in the finite element analysis as summarized in Table 2, that is, flexural failure (F) and flexural-shear failure

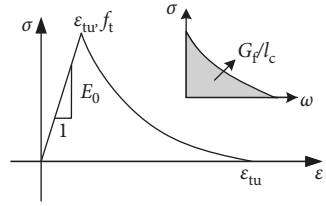

Figure 4: Tensile stress-strain curve of concrete.

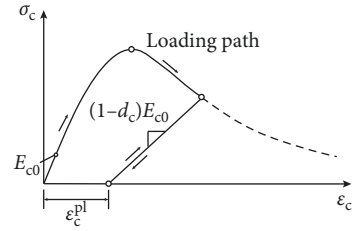

Figure 5: Stress-strain relation for cyclic compressive loading.

(FS). Figures 7(a)–7(c) demonstrate the predicted and test concrete damage of specimen GB2-3-1 which shows a typical flexural failure. As shown in Figure 7(a), bottom concrete of boundary columns suffered the most severe compressive damage, which can be observed in the test as shown in Figure 7(c). Specimen W1-a failed in a flexural and shear failure mode. Obvious shear cracks developed along the height of the shear wall, and the bottom concrete crushed under flexural and shear effects, as the test failure mode of specimen W1-a shown in Figure 8(c). This can be confirmed in the FE results shown in Figures 8(a) and 8(b).

3. Deformation Capacity of SPRC Shear Wall

Ductility is an important index of deformation capacity of members and structures in displacement-based design. Generally, ductility of members is represented by ductility factor defined as the ratio of ultimate displacement to yield displacement. Based on the test specimen in reference [7], 720 finite element models of the SPRC shear wall with potential flexural failure were developed. The typical section is shown in Figure 9. The main parameters of the FEMs are listed in Table 4.

The load history in most tests [5–7] begins with force-controlled elastic cycles to the predicted yield force, followed by displacement-controlled cycles incremented by multiple of yield displacement. According to Rahnavard et al. [9], a simplified displacement-controlled scheme is adopted to generate cyclic behavior of SPRC shear walls with different shear span ratios. The typical loading protocol is shown in Figure 10, which is represented by the drift angle defined as the lateral displacement divided by the total height of the specimen.

The yield strength and ultimate strength of steel and rebars are determined from the experiment, detailed values listed in Table 5. Cyclic analyses were conducted in ABAQUS. Then, the yield displacement and ultimate displacement were obtained in the same way above.

Table 1: Detailed parameters of specimens.

Ref.	Test no.	$h_w \times l_w \times t_w$ (mm)	n	λ	f_c (Mpa)	Web			Boundary member	
						f_{yt} (MPa); ρ_t (%)	f_{yl} (MPa); ρ_l (%)	f_{yp} (MPa); ρ_p (%)	f_{ys} (MPa); ρ_s (%)	f_{ya} (MPa); ρ_a (%)
Wu [5]	W1-a	1200 × 800 × 80	0.5	1.5	66	409, 0.94	409, 0.35	416, 2.5	409, 9.24	416, 3.14
	W1-b	1200 × 800 × 80	0.5	1.5	66	409, 0.94	409, 0.35	416, 1.0	409, 9.24	416, 3.14
	W1-c	1200 × 800 × 80	0.5	1.5	66	409, 0.94	409, 0.35	416, 1.5	409, 9.24	416, 3.14
Jiang [6]	SPRCW1	2100 × 800 × 150	0.42	2.7	69	291, 0.67	298, 0.38	310, 3.33	440, 0.68	334, 1.26
	SPRCW2	2100 × 800 × 150	0.5	2.7	69	291, 0.67	298, 0.38	310, 3.33	440, 0.68	334, 1.26
	SPRCW3	2100 × 800 × 150	0.58	2.7	69	291, 0.67	298, 0.38	310, 3.33	440, 0.68	334, 1.26
Zhu [7]	GB2-3-1	1500 × 1000 × 125	0.25	2	67	576, 0.59	576, 0.59	330, 2.5	475, 2.18	353, 5.70
	GB2-3-2	1500 × 1000 × 125	0.3	2	64	576, 0.59	576, 0.59	330, 2.5	475, 2.18	353, 5.70
	GB2-3-3	1500 × 1000 × 125	0.3	2	60	498, 0.59	498, 0.59	330, 2.5	475, 2.18	353, 5.70

h_w, l_w, and t_w are the height, length, and thickness of the composite shear wall; the concrete cylinder compressive strength f_c is taken as $0.76f_{cu}$ for C50, $0.82f_{cu}$ for C80 and f_{cu} multiplied by the linear interpolation between 0.76 and 0.82 for concrete with strength grade between C50 and C80; n is the axial load ratio; λ is the shear span ratio; f_{yt}, f_{yl}, f_{yp}, ρ_t, ρ_l, and ρ_p are the yield strengths and ratios of the transverse, longitudinal reinforcement, and steel plate of the wall web; f_{ys}, f_{ya}, ρ_s, and ρ_a are the yield strengths and ratios of the longitudinal reinforcement and structural steel of the boundary members.

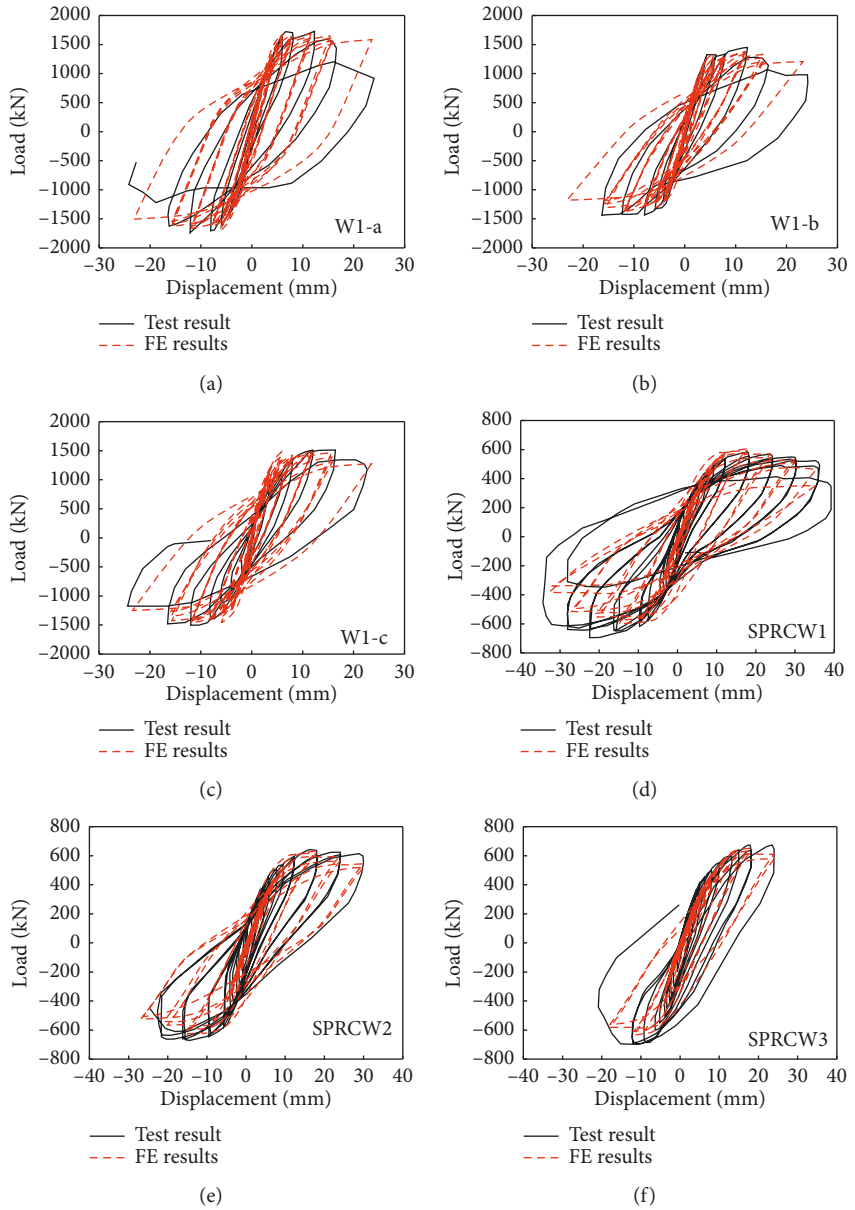

Figure 6: Continued.

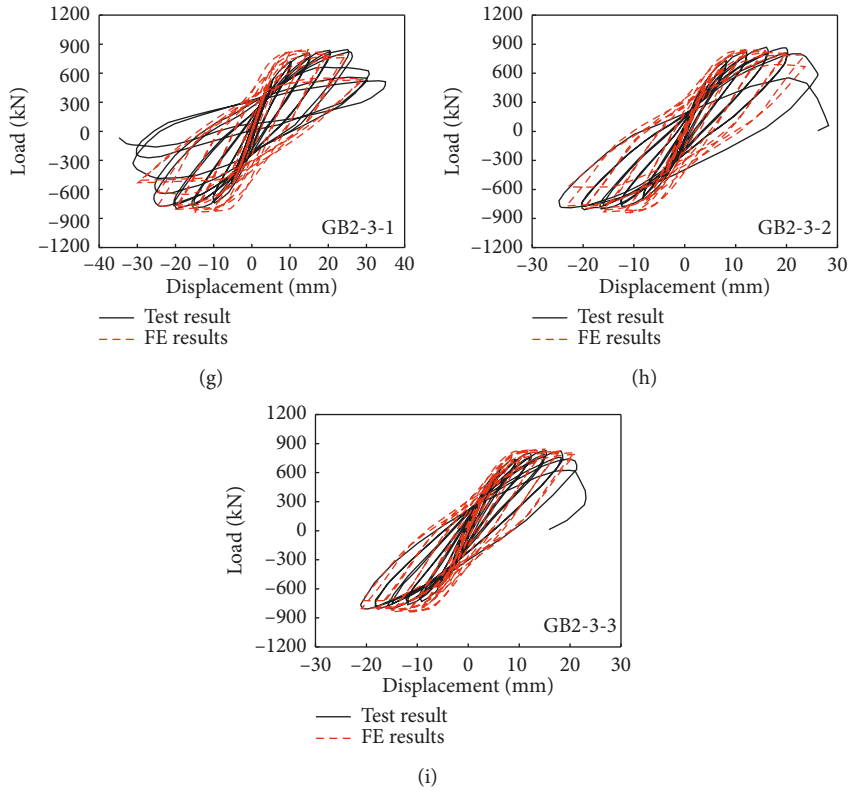

Figure 6: Comparison of displacement-force relation between tests and finite element results. (a) W1-a; (b) W1-b; (c) W1-c; (d) SPRCW1; (e) SPRCW2; (f) SPRCW3; (g) GB2-3-1; (h) GB2-3-2; (i) GB2-3-3.

Table 2: Comparison of strengths between tests and finite element results.

Ref.	Test no.	Yield load (kN)		Q_{TEST}/Q_{FEM}	Peak load (kN)		P_{TEST}/P_{FEM}	Failure mode	
		Q_{TEST}	Q_{FEM}		P_{TEST}	P_{FEM}		Test	FEM
Wu [5]	W1-a	1520.00	1509.30	1.01	1730.00	1696.08	1.02	FS	FS
	W1-b	1120.00	1178.40	0.95	1450.00	1380.95	1.05	FS	FS
	W1-c	1214.00	1248.90	0.97	1515.00	1470.88	1.03	FS	FS
Jiang [6]	SPRCW1	542.50	552.30	0.98	638.80	604.80	1.06	F	F
	SPRCW2	555.20	555.90	1.00	659.70	633.90	1.04	F	F
	SPRCW3	570.70	566.70	1.00	687.70	651.80	1.06	F	F
Zhu [7]	GB2-3-1	607.00	630.10	0.96	828.00	840.10	0.99	F	F
	GB2-3-2	613.00	633.20	0.97	841.00	844.20	1.00	F	F
	GB2-3-3	612.00	631.00	0.97	822.00	841.30	0.98	F	F
Mean value		—	—	0.95	—	—	1.03	—	—
Standard variation σ		—	—	0.05	—	—	0.05	—	—

3.1. Yield Rotation of SPRC Shear Wall. Slender shear wall tends to be dominated by flexural failure. The yielding of a cantilever shear wall occurs when its bottom section yields, when the curvature is linearly distributed along the height of the wall. The curvature of the top section is 0. The yield curvature is taken as ϕ_y, and then the yield displacement of shear wall is

$$\theta_y = \frac{1}{3}\phi_y H, \tag{18}$$

where H is the height of the shear wall.

Priestley [22] suggests that the yield curvature of the shear wall is only relevant to the yield strain of tensile longitudinal reinforcement ε_y and the section depth h_w:

$$\phi_y = \frac{a f_y}{E_s h_w}. \tag{19}$$

The yield rotation of the shear wall is given in the form where a is an undetermined coefficient:

$$\theta_y = \frac{a}{3}\frac{f_y}{E_s h_w} H. \tag{20}$$

By ignoring shear deformation, the yield rotation is defined as

$$\theta_{y,FEM} = \frac{\Delta_{y,FEM}}{H}. \tag{21}$$

Table 3: Comparison of deformation capacity between tests and finite element results.

Ref.	Test no.	Δ_y (mm)		$\Delta_{y,TEST}/\Delta_{y,FEM}$	Δ_u (mm)		$\Delta_{u,TEST}/\Delta_{u,FEM}$	μ		μ_{TEST}/μ_{FEM}
		$\Delta_{y,TEST}$	$\Delta_{y,FEM}$		$\Delta_{u,TEST}$	$\Delta_{u,FEM}$		μ_{TEST}	μ_{FEM}	
Wu [5]	W1-a	4.32	4.99	0.87	17.80	23.20	0.77	4.12	4.65	0.89
	W1-b	3.57	4.40	0.81	13.80	23.18	0.60	3.87	5.27	0.73
	W1-c	5.35	4.54	1.18	21.25	23.28	0.91	3.97	5.13	0.77
Jiang [6]	SPRCW1	8.60	6.99	1.23	33.90	29.10	1.16	3.93	4.16	0.94
	SPRCW2	6.90	7.00	0.99	26.65	27.03	0.99	3.93	3.86	1.02
	SPRCW3	8.00	7.12	1.12	20.42	20.90	0.98	2.69	2.94	0.92
Zhu [7]	GB2-3-1	6.92	6.32	1.09	27.22	26.04	1.05	3.96	4.12	0.96
	GB2-3-2	6.13	6.54	0.94	25.45	23.65	1.08	4.15	3.62	1.15
	GB2-3-3	6.10	6.09	1.00	21.41	20.96	1.02	3.51	3.44	1.02
Mean value		—	—	1.05	—	—	1.07	—	—	1.03
Standard variation, σ		—	—	0.09	—	—	0.06	—	—	0.08

Δ_y is the yield displacement of the specimen; Δ_u is the ultimate displacement of the specimen; μ is the ductility factor defined by the ratio of ultimate displacement to yield displacement.

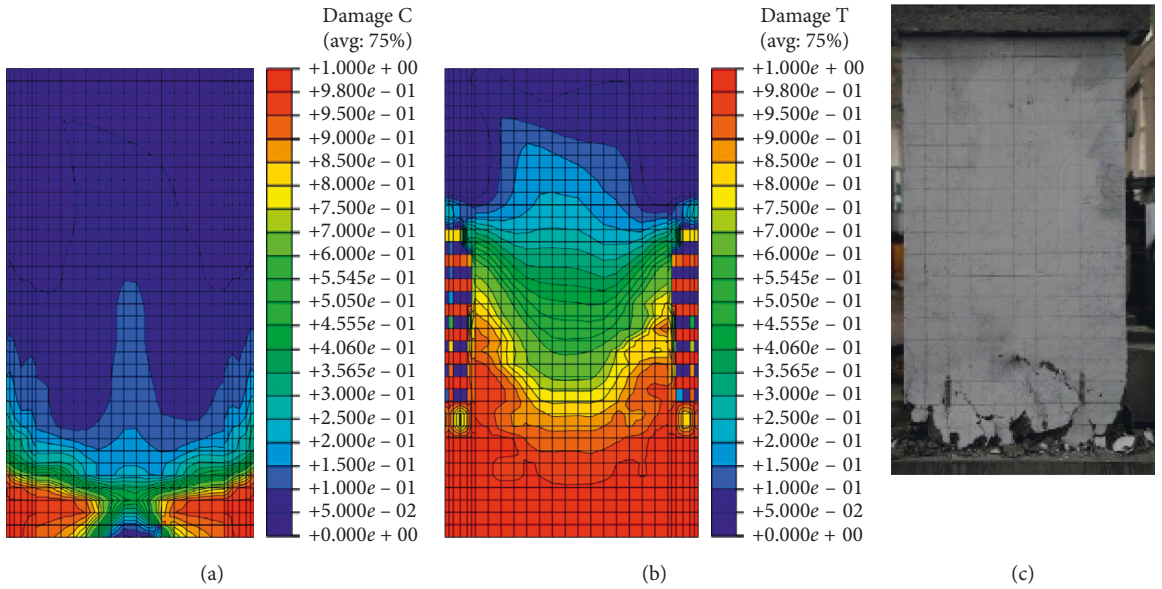

Figure 7: Predicted and test concrete damage of specimen GB2-3-1. (a) Concrete compressive damage. (b) Concrete tensile damage. (c) Test failure.

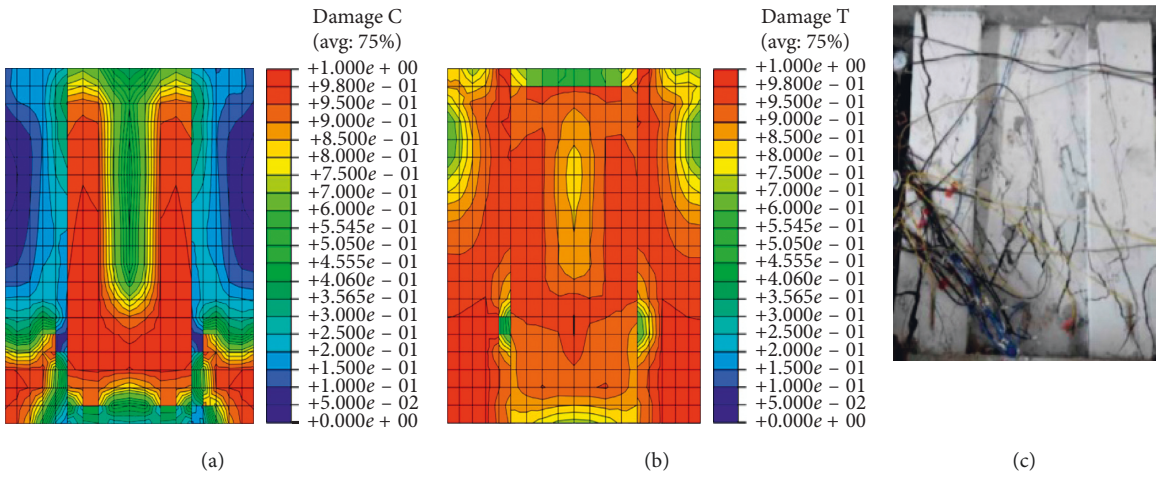

Figure 8: Predicted and test concrete damage of specimen W1-a. (a) Concrete compressive damage. (b) Concrete tensile damage. (c) Test failure.

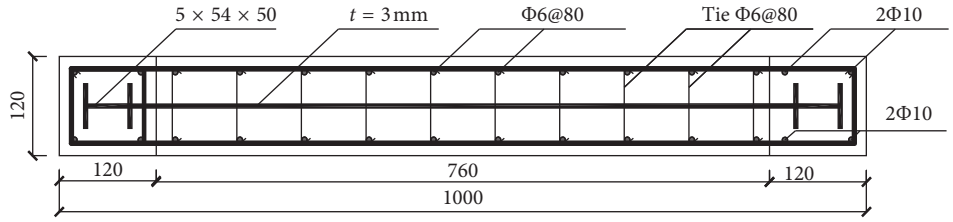

Figure 9: Typical section of the parametric study.

Table 4: Parameters of finite element models.

Parameter	Values
Shear span ratio	2.5, 3.0, 3.5
Concrete cylinder compressive strength (MPa)	32.4, 38.5, 44.5, 50.2
Axial load ratio	0.2, 0.3, 0.4
Transverse reinforcement ratio (%)	0.3, 0.4, 0.6, 0.8, 0.95
Steel plate ratio	0.01, 0.03, 0.05, 0.07

The coefficient a is determined by regression analyses of finite element results. Then, the yield curvature and rotation are given by

$$\phi_y = \frac{3.35 f_y}{E_s h_w}, \tag{22}$$

$$\theta_y = \frac{1.12 f_y H}{E_s h_w}. \tag{23}$$

The ratios of yield rotation calculated from finite element analyses and proposed formula are shown in Figure 8, with a mean value of 1.00 and coefficient of variation (C.V) of 33.4%. Results of shear walls with different steel plate ratios and axial load ratios are marked to illustrate the effect of these parameters. Experiment results suggest that the yield and ultimate deformations of the SPRC shear wall are improved compared with those of the steel reinforced concrete composite shear wall. The yield rotation tends to rise as the steel plate ratio increases, which can be seen in Figure 11(a). No obvious effect of axial load ratio is found on yield rotation of SPRC shear walls.

3.2. Ultimate Rotation of SPRC Shear Wall. The ultimate rotation can be calculated on the basis of purely flexural behavior by the concept of plastic hinge and plastic hinge length L_p for the slender shear wall [14]. The plastic hinge assumes that the plastic curvature ϕ_p is lumped and uniformly distributed in the plastic hinge length, where $\phi_p = \phi_u - \phi_y$. The ultimate rotation is calculated by

$$\theta_u = \frac{1}{3}\phi_y H + \left(\phi_u - \phi_y\right) L_p \left(1 - \frac{0.5 L_p}{H}\right), \tag{24}$$

where ϕ_p and ϕ_u are the yield curvature and ultimate plastic curvature of the bottom section, respectively.

Priestley and Paulay [23] suggest that the plastic hinge length L_p of the shear wall is related to its section depth and the height:

$$L_p = 0.2 h_w + 0.044 H, \tag{25}$$

where h_w is the section depth and H is the height of the shear wall.

It is assumed that the plastic hinge fails when the compressive zone of the concrete reaches the ultimate concrete strain. The Mander model, as simplified by Paulay and Priestley [23] regarding the calculation of the ultimate strain of confined concrete, was applied:

$$\varepsilon_{cu} = 0.004 + 1.4 \varepsilon_{su} \frac{\rho_s f_{yw}}{f_{cc}}, \tag{26}$$

where ε_{su} is the elongation at steel rupture, ρ_s is the volumetric ratio of confining steel, f_{yw} is the yield strength of confining steel, and f_{cc} is the compressive strength of confined concrete. According to Jiang, ε_{su} is taken as 0.12.

On the basis of the plane-section hypothesis, the compressive section depth x_n and the corresponding relative compressive section depth ξ_u are determined by the force balance which is shown in Figure 12.

For the SPRC shear wall of the rectangular section, the force balance is

$$0.8 f_c b_w x_n + f'_a A'_a + f'_y A'_s = f_a A_a + f_s A_s + N_{sw} + N_{sp} + N, \tag{27}$$

where

$$N_{sp} = (h_w - 2x_n) t_{sp} f_p, \tag{28}$$

$$N_{sw} = \frac{(h_w - 2x_n) A_{sw} f_{yw}}{(h_w - 2x_w)}. \tag{29}$$

Then, the relative compressive section depth of concrete is

$$\xi_n = \frac{\rho_a f_a + \rho f_y - \rho'_a f'_a + \rho' f'_y + \rho_p f_p + \rho_{sw} f_{yw} + N/b_w h_w}{0.8 f_c + 2\rho_p f_p + 2\rho_{sw} f_{yw}}, \tag{30}$$

where A_s, A'_s, ρ, ρ', f_y, and f'_y are the areas, reinforcement ratio, and yield strength of tensile and compressive rebar of the boundary members of the shear wall, respectively; A_a, A'_a, ρ_a, ρ'_a, f_a, and f'_a are the areas, reinforcement ratios, and yield strength of tensile and compressive structural steel of boundary members, respectively; ρ_p is the steel plate ratio,

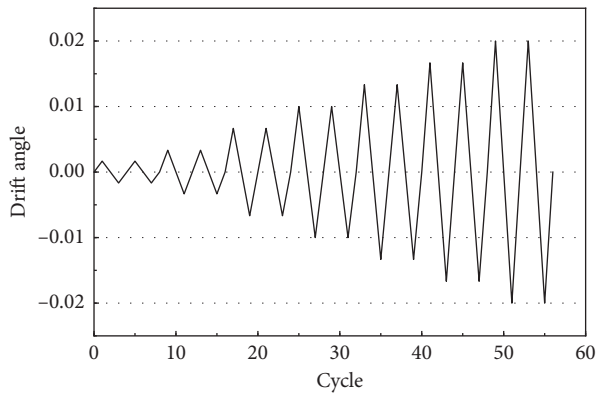

Figure 10: Loading protocol of the numerical analyses.

Table 5: Strengths of steel and rebars.

Material	Yield strength (MPa)	Ultimate strength (MPa)	Elastic modulus (MPa)
Structural steel	353	460	2.06×10^5
Steel plate	330	457	2.06×10^5
Rebar D6	498	718	2.10×10^5
Rebar D10	475	694	2.10×10^5

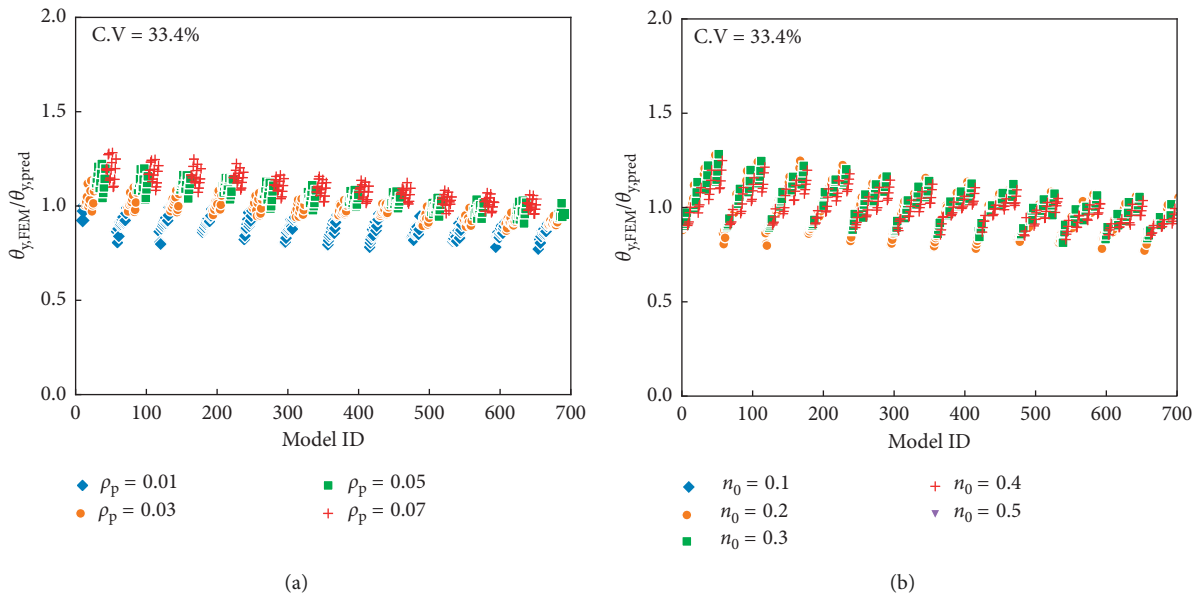

Figure 11: Distribution of yield rotations. (a) Different steel plate ratios. (b) Different axial load ratios.

where $\rho_{sp} = t_{sp}/b_w$; ρ_{sw} is the longitudinal reinforcement ratio of the shear wall web; f_p and f_{yw} are the yield strengths of steel plate and rebars of the wall web. N is the axial load; and N_{sp} and N_{sw} are the axial force resisted by steel plate and reinforcement of the wall web, respectively.

The ultimate curvature is calculated by the ratio of the ultimate strain to the compressive section depth:

$$\phi_u = \frac{\varepsilon_{cu}}{x_n}. \tag{31}$$

By substituting equations (23), (25), (26), and (31), the ultimate rotation is

$$\theta_u = \frac{1.12 f_y H}{E_s h_w} + \left(\frac{0.004 + 0.168\lambda_{sv}}{x_n} - \frac{3.35 f_y}{E_s h_w}\right)(0.2h_w + 0.044H). \tag{32}$$

The predicted ultimate rotation $\theta_{u,pred}$ calculated by using equation (32) is compared with the numerical ultimate rotation $\theta_{u,FEM}$ in Figure 13. The mean value of the ratio of numerical to predicted values $\theta_{u,FEM}/\theta_{u,pred}$ is 1.08, with the coefficient of variation of 18.9%.

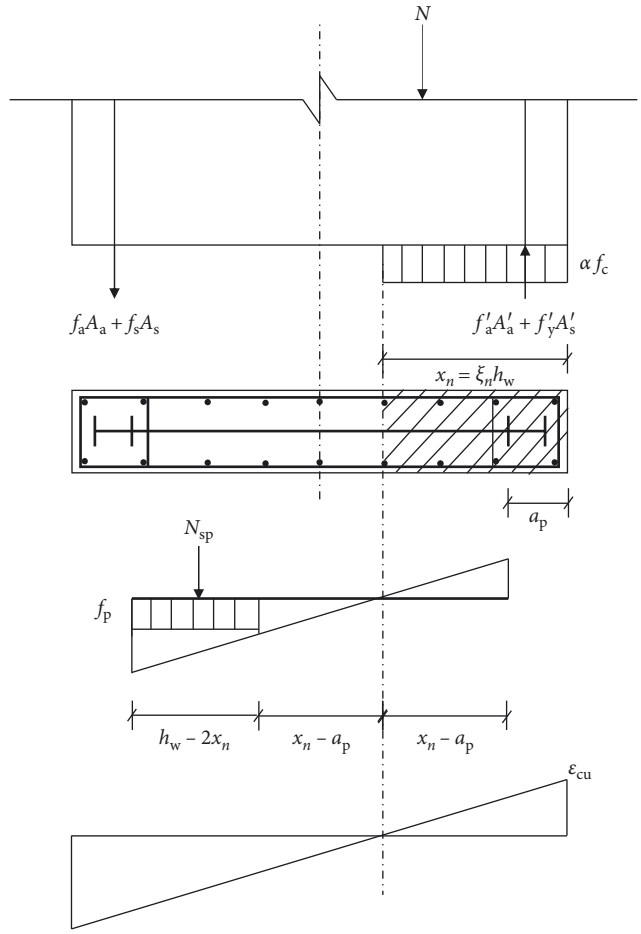

Figure 12: Compressive section depth of concrete.

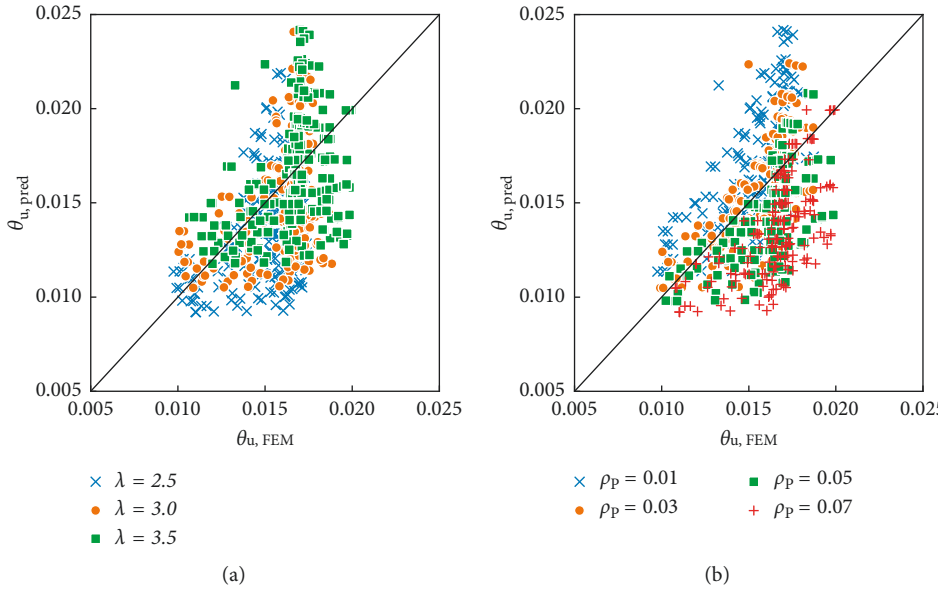

Figure 13: Continued.

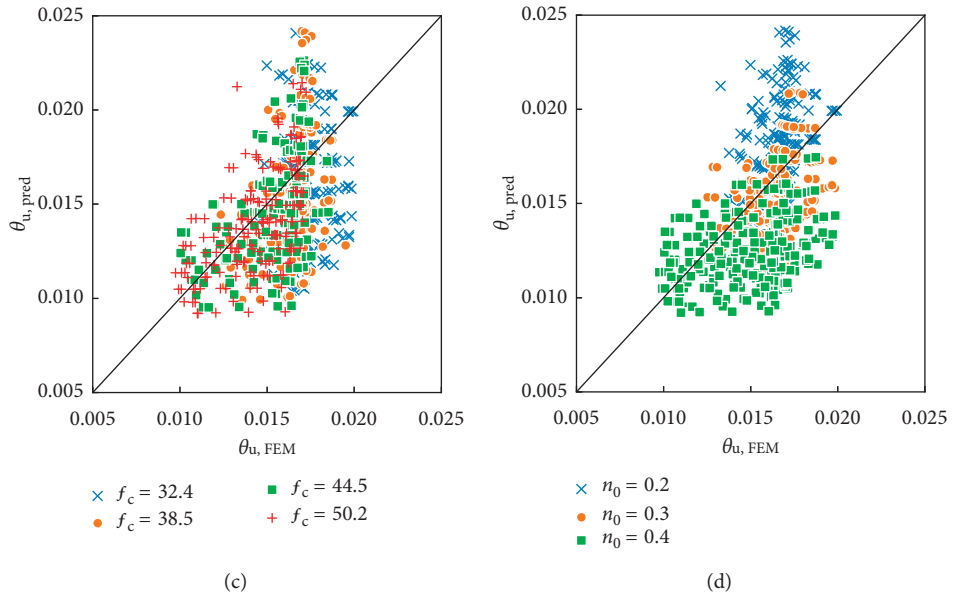

Figure 13: Distribution of numerical and predicted ultimate rotation. (a) Different shear span ratios. (b) Different steel plate ratios. (c) Different concrete grades. (d) Different axial load ratios.

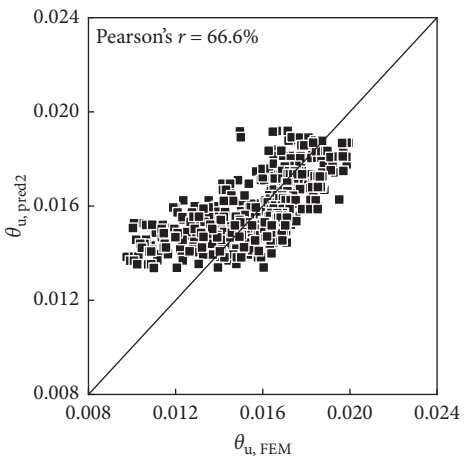

Figure 14: Numerical and predicted ultimate rotation.

Table 6: Comparison of deformation capacity between tests and predicted results.

Ref.	Test no.	Δ_y (mm)		$\Delta_{y,TEST}/\Delta_{y,pred}$	Δ_u (mm)		$\Delta_{u,TEST}/\Delta_{u,pred}$	μ		μ_{TEST}/μ_{pred}
		$\Delta_{y,TEST}$	$\Delta_{y,pred}$		$\Delta_{u,TEST}$	$\Delta_{u,pred}$		μ_{TEST}	μ_{pred}	
Jiang [6]	SPRCW1	8.60	7.89	1.09	33.90	28.50	1.19	3.94	3.61	1.09
	SPRCW2	6.90	7.89	0.87	26.65	26.40	1.01	3.86	3.35	1.15
	SPRCW3	8.00	7.89	1.01	20.42	24.70	0.83	2.55	3.13	0.81
Zhu [7]	GB2-3-1	6.92	6.43	1.08	27.22	25.60	1.06	3.93	3.98	0.99
	GB2-3-2	6.13	6.43	0.95	25.45	23.90	1.06	4.15	3.72	1.12
	GB2-3-3	6.10	6.43	0.95	21.41	24.30	0.88	3.51	3.78	0.93
	GB2-3-4	6.80	6.43	1.06	22.59	23.10	0.98	3.32	3.59	0.93
	GB2-5-1	6.61	6.43	1.03	28.39	23.60	1.20	4.29	3.67	1.17
	GB2-5-2	8.02	6.43	1.25	24.77	21.40	1.16	3.09	3.33	0.93
	GB2-5-3	6.84	6.43	1.06	24.64	21.80	1.13	3.60	3.39	1.06
	GB2-5-4	6.36	6.43	0.99	18.49	21.90	0.84	2.91	3.41	0.85

Table 6: Continued.

Ref.	Test no.	Δ_y (mm)		$\Delta_{y,TEST}/\Delta_{y,pred}$	Δ_u (mm)		$\Delta_{u,TEST}/\Delta_{u,pred}$	μ		μ_{TEST}/μ_{pred}
		$\Delta_{y,TEST}$	$\Delta_{y,pred}$		$\Delta_{u,TEST}$	$\Delta_{u,pred}$		μ_{TEST}	μ_{pred}	
Chen [24]	SRCW3-1a	7.60	6.96	1.09	42.95	36.40	1.18	5.65	5.23	1.08
	SRCW3-1b	7.10	6.96	1.02	34.55	36.40	0.95	4.87	5.23	0.93
	SRCW3-2a	7.15	6.96	1.03	32.85	33.70	0.97	4.59	4.84	0.95
	SRCW3-2b	6.45	6.96	0.93	34.95	33.70	1.04	5.42	4.84	1.12
	SRCW3-3a	6.50	6.96	0.93	32.70	30.70	1.07	5.03	4.41	1.14
	SRCW3-3b	7.15	6.96	1.03	34.15	30.70	1.11	4.78	4.41	1.08
Mean value		—	—	1.02	—	—	1.04	—	—	1.01
Standard variation, σ		—	—	0.08	—	—	0.11	—	—	0.11

As shown in Figure 9, $\theta_{u,FEM}/\theta_{u,pred}$ is similarly distributed under different shear span ratios and concrete grades, while the ratio tends to degrade as the steel plate ratio and axial load ratio increase because the compressive section depth is affected by the steel plate ratio and axial load. For a slender shear wall with the plane-section hypothesis, a larger axial load ratio will increase the compressive section depth of concrete and consequently decrease the ultimate curvature. Equation (32) tends to underestimate the compressive section depth of the shear wall with a small steel plate ratio and axial load ratio. To simplify the statistical procedure, equation (32) is transformed into a simple formula that includes the main variables, that is, compressive section depth, characteristic volumetric value of the boundary member, and shear span ratio:

$$\theta_u = \frac{C_0(\lambda_{sv} + C_1)(H/h_w)^{C_2}}{(\xi_u + C_3)}, \tag{33}$$

where C_0, C_1, C_2, and C_3 are undetermined coefficients.

The numerical values of the ultimate rotation are used to determine the coefficients by regression analyses:

$$\theta_u = \frac{0.356(\lambda_{sv} + 0.1)(H/h_w)^{0.278}}{(\xi_u + 4.89)}. \tag{34}$$

Numerical values of θ_u are compared with the predictions by equation (34) $\theta_{u,pred2}$ in Figure 14. The mean value of the ratios of numerical to predicted values $\theta_{u,FEM}/\theta_{u,pred2}$ is 1.00, with the coefficient of variation of 9.9%. The maximum and minimum ratios are 1.2 and 0.64, respectively.

The deformation capacities predicted by using equations (23) and (34) are compared with test results [6–8] in Table 6. The mean value of the ratios of the test to predicted yield deformations $\Delta_{y,TEST}/\Delta_{y,pred}$ is 1.02, with the coefficient of variation of 8.3%. The mean value of the ratios of the test to predicted ultimate deformations $\Delta_{u,TEST}/\Delta_{u,pred}$ is 1.04, with the coefficient of variation of 11.5%. A good agreement is achieved between the test and predicted deformation capacities of SPRC shear walls.

4. Conclusions

This paper investigates the deformation capacity of SPRC shear walls under cyclic loads. A nonlinear 3-D finite element model in ABAQUS was developed and validated against published experimental results. Then, a parametric study was conducted to obtain the yield rotation and ultimate rotation of SPRC shear walls with potential flexural failure. By statistical analyses, formulas for the yield rotation and ultimate rotation for SPRC shear walls are proposed. The cyclic behavior of SPRC shear walls can be predicted by using these formulas and related studies on shear capacities and hysteretic models [7–10], which can be used by engineers to conduct a displacement-based performance design of SPRC shear wall system.

The proposed formulas focused on SPRC shear walls with high shear span ratio and flexure-dominated behavior in which shear studs are well distributed according to the Chinese code for design of composite structures. Further work will involve the SPRC shear walls with low shear span ratio and different configurations of shear connectors.

Data Availability

The data used to support the findings of this study are available from the corresponding author upon request.

Conflicts of Interest

The authors declare that there are no conflicts of interest regarding the publication of this paper.

Acknowledgments

The financial support provided by the National Key Research and Development Program of China (Grant no. 2017YFC1500701), the National Natural Science Foundation of China (Grant nos. 51638016 and 51608406), and the Fundamental Research Funds for the Central Universities (WUT: 2018IVB013) is gratefully acknowledged.

References

[1] A. Astaneh-Asl, *Seismic Behavior and Design of Composite Steel Plate Shear Walls*, Moraga, CA, USA, Structural Steel Educational Council, 2002.

[2] American Institute of Steel Construction, *Seismic Provisions for Structural Steel Buildings*, American Institute of Steel Construction, Chicago, IL, USA, 2002.

[3] Q. Zhao and A. Astaneh-Asl, "Cyclic behavior of traditional and innovative composite shear walls," *Journal of Structural Engineering*, vol. 130, no. 2, pp. 271–284, 2004.

[4] C. J. Gan, X. L. Lu, and W. Wang, "Seismic behavior of steel plate reinforced concrete shear walls," in *Proceedings of the*

14th World Conference on Earthquake Engineering, Beijing, China, October 2008.

[5] X. C. Wu, "Study on seismic behavior of composite shear wall with high strength concrete and infill steel plates," Master's thesis, South China University of Technology, Guangzhou, China, 2014.

[6] D. Q. Jiang, "Experimental research on press-bending behavior of high-strength concrete steel composite walls," Master's thesis, China Academy of Building Research, Beijing, China, 2011.

[7] A. P. Zhu, *Seismic behavior of embedded steel plate reinforced C80 concrete composite shear walls*, Ph.D. dissertation, China Academy of Building Research, Beijing, China, 2015.

[8] W. Wang, Y. Wang, and Z. Lu, "Experimental study on seismic behavior of steel plate reinforced concrete composite shear wall," *Engineering Structures*, vol. 160, pp. 281–292, 2018.

[9] R. Rahnavard, A. Hassanipour, and A. Mounesi, "Numerical study on important parameters of composite steel-concrete shear walls," *Journal of Constructional Steel Research*, vol. 121, pp. 441–456, 2016.

[10] B. Wang, H. Jiang, and X. Lu, "Seismic performance of steel plate reinforced concrete shear wall and its application in China mainland," *Journal of Constructional Steel Research*, vol. 131, pp. 132–143, 2017.

[11] E. Ellobody and B. Young, "Design and behaviour of concrete-filled cold-formed stainless steel tube columns," *Engineering Structures*, vol. 28, no. 5, pp. 716–728, 2006.

[12] E. Ellobody and B. Young, "Nonlinear analysis of concrete-filled steel SHS and RHS columns," *Thin-Walled Structures*, vol. 44, no. 8, pp. 919–930, 2006.

[13] T. Yu, J. G. Teng, Y. L. Wong, and S. L. Dong, "Finite element modeling of confined concrete-II: plastic-damage model," *Engineering Structures*, vol. 32, no. 3, pp. 680–691, 2010.

[14] Fib, *Fib Model Code for Concrete Structures 2010*, International Federation for Structural Concrete, Berlin, Germany, 2013.

[15] J. B. Mander, M. J. N. Priestley, and R. Park, "Theoretical stress-strain model for confined concrete," *Journal of Structural Engineering*, vol. 114, no. 8, pp. 1804–1826, 1988.

[16] M. D. Denavit, J. F. Hajjar, and R. T. Leon, "Seismic behavior of steel reinforced concrete beam-columns and frames," in *Proceedings of the Structures Congress 2011*, pp. 2852–2861, Las Vegas, NV, USA, April 2011.

[17] W. Huang, Z. Zhou, and J. Liu, "Analytical deformation characteristics and shear capacity of SRC-RC transfer columns," *Journal of Constructional Steel Research*, vol. 138, pp. 692–700, 2017.

[18] S. Popovics, "A numerical approach to the complete stress-strain curve of concrete," *Cement and Concrete Research*, vol. 3, no. 5, pp. 583–599, 1973.

[19] M. P. Collins, D. Mitchell, and J. G. MacGregor, "Structural design considerations for high-strength concrete," *Concrete International*, vol. 15, no. 5, pp. 27–34, 1993.

[20] ACI, *Building Code Requirements for Structural Concrete and Commentary (ACI 318-11)*, American Concrete Institute, Farmington Hills, MI, USA, 2011.

[21] V. Birtel and P. Mark, "Parameterised finite element modelling of RC beam shear failure," in *Proceedings of the ABAQUS Users' Conference*, pp. 95–108, Boston, MA, USA, May 2006.

[22] M. J. N. Priestley, "Direct displacement-based design of precast/prestressed concrete buildings," *PCI Journal*, vol. 47, no. 6, pp. 66–79, 2002.

[23] M. J. N. Priestley and T. Paulay, *Seismic Design of Reinforced Concrete and Masonry Buildings*, New York, NY, USA, John Wiley & Sons, Inc., 1992.

[24] T. Chen, C. Z. Xiao, C. Y. Tian, and P. F. Xu, "Experimental study of the compression-bending behavior of composite shear walls of high axial compression ratios," *China Civil Engineering Journal*, vol. 44, no. 6, pp. 1–7, 2011.